Absence of localization in weakly interacting Floquet circuits

Dominik Hahn[1,*] and Luis Colmenarez[1,2,3,†]

[1]*Max Planck Institute for the Physics of Complex Systems, Nöthnitzer Straße 38, 01187-Dresden, Germany*

[2]*Institute for Quantum Information, RWTH Aachen University, 52056 Aachen, Germany*

[3]*Institute for Theoretical Nanoelectronics (PGI-2), Forschungszentrum Jülich, 52428 Jülich, Germany*

(Received 22 November 2023; revised 7 March 2024; accepted 7 March 2024; published 21 March 2024)

We present a family of Floquet circuits that can interpolate between noninteracting qubits, free propagation, generic interacting, and dual-unitary dynamics. We identify the operator entanglement entropy of the two-qubit gate as a good quantitative measure of the interaction strength. We test the persistence of localization in the vicinity of the noninteracting point by probing spectral statistics, decay of autocorrelators, and measuring entanglement growth. The finite-size analysis suggests that the many-body localized regime does not persist in the thermodynamic limit. Instead, our results are compatible with an integrability-breaking phenomenon.

DOI: 10.1103/PhysRevB.109.094207

I. INTRODUCTION

Thermalization of quantum many-body systems has been an active topic of research in recent years [1–3]. It is now known that generic interacting systems reach an equilibrium state that can be described by a statistical mechanics ensemble [4–6]. Such systems show quantum chaotic dynamics, which encompasses several dynamical and static traits [7,8]. There are two nongeneric cases where the dynamics is not expected to be chaotic: (i) Noninteracting systems can show free propagation or get localized in the presence of disorder, the latest being called Anderson localization [9]. (ii) Interacting integrable systems whose extensive number of conserved quantities constrained their dynamics, giving rise to a special type of thermalization [10]. When integrability is perturbed in an extensive manner, quantum chaos is expected to set in the long run and the system thermalizes [8,11–14]. However, in recent years, it was shown that strong disorder potentials may cause the breakdown of thermalization, the so-called many-body localization (MBL) [15–17]. This is described as an ergodicity-breaking transition at finite interaction strength and disorder. In this regime, quasilocal conserved quantities [18,19] are stabilized, leading to emergent integrability out of an initially quantum chaotic system. There are lots of evidence of MBL in systems of moderate size [20,21] but, recently, the fate of MBL in the thermodynamic limit has been put into question [22–25] and spark debates on the scaling of the critical disorder and possible delocalization mechanisms [26–32].

An interesting question arises at the intersection of the dynamical regimes exposed above: How stable are Anderson localized systems to small interactions? On the one hand, any small interactions are expected to drive the system towards thermal equilibrium, on the other hand, disorder may overcome the interactions and the system becomes MBL. In Ref. [33] the authors studied a model where the MBL persists at small enough interactions. The critical value of the localization length is the one expected from the avalanche mechanism [34,35]. In Ref. [36] it is shown that small interactions are not effectively perturbing the Anderson localized orbitals when the disorder strength is large. In this work, we study the localization and delocalization transition in a maximally localized system subjected to small and medium-strength interactions.

Most of the studies that address the strong disorder and weak interaction limit focus on Hamiltonian systems so far. Here, we present a family of Floquet circuits that can interpolate between noninteracting qubits and strongly interacting systems. In this work, we carefully investigate the finite-size scaling of the putative localization-delocalization transition by analyzing various spectral and dynamical quantities [17,18,21,37–42]. Our results suggest that there exists no MBL phase for our system in the thermodynamic limit. Instead, our numerics suggest a finite-size crossover, reminiscent of integrability-breaking phenomena [43] in clean systems.

The structure of the paper is as follows: In Sec. II, we introduce our Floquet model and the quantities we use to study the onset of thermalization. In Sec. III, we present our results for various commonly studied quantities in the field, together with a finite-size scaling analysis. Finally in Sec. IV we discuss the implications and perspectives of our work.

II. MODEL AND OBSERVABLES

Before we present our results, we provide technical details about our model and different quantities to detect signatures of the MBL regime. In the following work, we study a family of

*hahn@pks.mpg.de

†colmenarez@physik.rwth-aachen.de

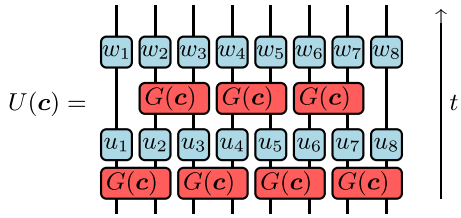

FIG. 1. Diagrammatic notation of the unitary defined in Eq. (3). The single-qubit gates u_i and w_i introduce spatial disorder to the system, while the interaction between neighboring qubit is mediated by the two-qubit gate $G(\mathbf{c})$.

Floquet models $U(\boldsymbol{c})$ shown in Fig. 1, defined by the three parameters $\boldsymbol{c} = (c_1, c_2, c_3)$. The single-qubit unitaries u_i and v_i are independently drawn from the Haar measure and introduce the spatial disorder of the model. The two-qubit gates $G(\boldsymbol{c})$ are determined by three parameters $\boldsymbol{c} = (c_1, c_2, c_3)$ and are fixed for the entire circuit. The two-qubit unitary $G(\boldsymbol{c})$ is defined in Sec. II A and it is shown there how it naturally appears in a classification of two-qubit gates.

After that, the family of Floquet models is introduced in Sec. II B, together with a description of special parameter choices $\boldsymbol{c}$ into the literature. Furthermore, we present a possible characterization for the "interaction strength" of two-qubit gates in terms of the gate operator entanglement in Sec. II C. This section is closed with a description of the various measures used in this work to characterize the finite-size scaling of the localization-delocalization transition in Secs. II D and II E.

A. Classification of two-qubit gates

For any two-qubit gate U_2, there exist general single-qubit gates u_1, u_2, v_1, and v_2 and a two-qubit gate of the form [with $\boldsymbol{c} = (c_1, c_2, c_3)$]

$$G(\boldsymbol{c}) = \exp\left[-i\frac{\pi}{2}(c_1\sigma^x \otimes \sigma^x + c_2\sigma^y \otimes \sigma^y + c_3\sigma^z \otimes \sigma^z)\right], \tag{1}$$

such that it can be decomposed as [44]

$$U_2 = (u_1 \otimes u_2)G(\boldsymbol{c})(v_1 \otimes v_2). \tag{2}$$

Here σ^α with $\alpha = x, y, z$ are the Pauli operators acting on each qubit.

Restricting to the subset $0.5 \geqslant c_1 \geqslant c_2 \geqslant c_3 \geqslant 0$, this allows for a classification of all two-qubit gates in terms of the vector $\boldsymbol{c}$: Two gates which are described by the same vector $\boldsymbol{c}$ are equivalent to each other up to single-qubit gates [45,46].

The space enclosed by the independent set of $\mathbf{c}$ is known as the Weyl chamber [47–49] and indicated by the purple tetrahedron in Fig. 2. There are a few special points and lines [45] (see Fig. 2):

(1) $c_1 = c_2 = c_3 = 0$ corresponds to independent single-qubit rotations.

(2) $c_1 = c_2 = c_3 = 0.5$ is the equivalence class of the SWAP gate up to single-qubit rotations.

(3) $c_1 = c_2 = 0.5$ and $c_3 \geqslant 0$ denote the family of dual-unitary gates (shown as an orange line in Fig. 2).

(4) $c_1 = 0.5$ and $c_2 = c_3 = 0$ is the CNOT gate up to single-qubit rotations.

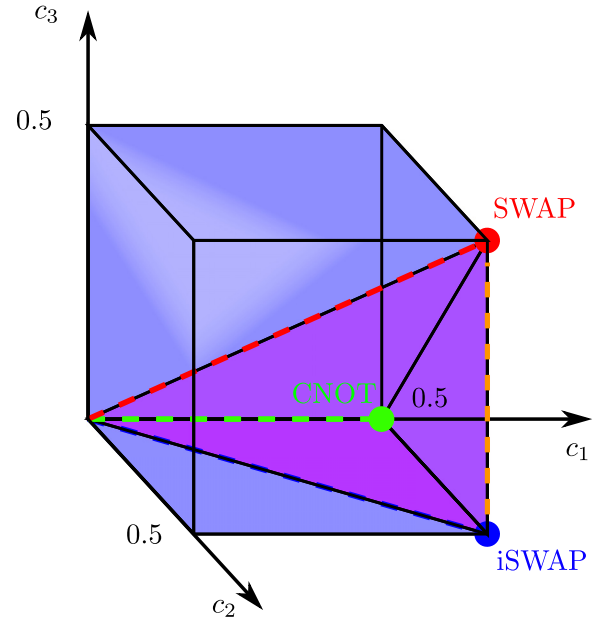

FIG. 2. Parametrization of different equivalence classes for two-qubit gates: Each two-qubit gate is uniquely determined up to single-qubit unitaries by three parameters $0 \leqslant c_3 \leqslant c_2 \leqslant c_1 \leqslant 0.5$ (purple tetrahedron) that form the Weyl chamber. Colored points indicate common gates. The dashed lines show the corresponding families of two-qubit gates defined in Sec. II B.

Since any two-qubit gate corresponds to a specific point of the Weyl chamber, the entanglement properties of each gate [Eq. (2)] are uniquely determined by the vector $\boldsymbol{c} = (c_1, c_2, c_3)$ [45,46,50], as will be illustrated in Sec. II C.

B. Floquet circuit model

The characterization of two-qubit unitaries by means of the gate $G(\mathbf{c})$ allows us to introduce the following family of Floquet circuits:

$$U(\boldsymbol{c}) = \prod_{i=0}^{L-1} w_i \prod_{k=0}^{L/2-2} G(\boldsymbol{c})_{2k+1,2k+2} \prod_{i=0}^{L-1} u_i \prod_{k=0}^{L/2-1} G(\boldsymbol{c})_{2k,2k+1}. \tag{3}$$

A diagrammatic representation of this circuit is shown in Fig. 1: the gates u_i and w_i are single-qubit rotations drawn from the Haar measure. They act as a spatial disorder. The gate $G(\boldsymbol{c})$ is defined in Eq. (1). All bonds have the same set of parameters $\boldsymbol{c} = (c_1, c_2, c_3)$. The Floquet dynamics is given by repeatedly applying U [Eq. (3)], thus, the Floquet circuit ensemble is determined by the vector $\boldsymbol{c}$.

A few special cases of this model have been already studied in the literature: The case of space-time dual-unitary circuits $c_1 = c_2 = 0.5$, $c_3 \geqslant 0$ (see orange dashed line in Fig. 2) has been extensively studied [51,52]. These circuits are quantum chaotic despite being exactly solvable, which makes them special in the study of thermalization [53–60]. For instance, they are shown to saturate bounds on information scrambling [57,61–63]. A random version of this circuit, different single-qubit gates at each time step, was studied in Ref. [64],

the authors found that the fastest scrambler quantum circuit, i.e., highest entanglement rate production, are random circuits with $c_1 = c_2 = 0.5$ and $c_3 \geqslant 0$.

The vicinity of the noninteracting point $c_1 = c_2 = c_3 = 0$ is less explored. A natural question is whether the system gets many-body localized [2,65] for small finite values of the coefficients (c_1, c_2, c_3). In principle, there are multiple possible choices for $\boldsymbol{c}$ that can be studied starting from the origin. We focus on three lines:

(1) SWAP line: it is determined by $c_1 = c_2 = c_3$ with $0 < c_1 < 0.5$ (see Fig. 2). It interpolates between single-qubit rotations ($c_1 = 0$) and the SWAP gate ($c_1 = 0.5$).

(2) CNOT line: denoted by $c_2 = c_3 = 0$ and $0 < c_1 < 0.5$, this line ends on a CNOT gate-based circuit.

(3) The imaginary SWAP (iSWAP) [66] line given by $c_3 = 0$, $c_1 = c_2$, and $0 < c_1 < 0.5$ that ends on the imaginary-SWAP gate $c_1 = c_2 = 0.5$.

In Ref. [67] the authors report MBL for small coefficients on the SWAP line. Aside from the three lines mentioned above, we study a subset $\mathbf{c} = (c_1, c_2, c_3)$ with $c_1, c_2 \in (0.02, 0.28)$ and $c_3 \in (0.0, 0.18)$ in order to test the generality of the chosen lines and possible links between long-time dynamics and two-qubit gate invariants.

C. Two-qubit gate entanglement

As mentioned in previous sections, a possible quantity to characterize the "interaction strength" in the introduced class of Floquet models is by means of their operator Schmidt decomposition [50]:

$$U_2 = \sum_{l=1}^{4} \lambda_l (A_l \otimes B_l), \tag{4}$$

where A_l and B_l are orthonormal operators for the corresponding single-qubit spaces. This is analogous to the Schmidt decomposition of states. The Schmidt coefficients λ_l are normalized, i.e., $\sum_{l=1}^{4} \lambda_l = 1$. It turns out that two-qubit gates [Eq. (2)] that are different only in single-qubit rotations will have the same set of Schmidt coefficients [50]. Henceforth, the set (c_1, c_2, c_3) uniquely determines any function of the Schmidt coefficients. In the following, we use the second Renyi entropy [45,50] which allows us to define the operator entanglement per gate as

$$s(\boldsymbol{c}) = -\ln\left(\sum_{l=1}^{4} \lambda_l^2\right). \tag{5}$$

There are a few remarks with respect to the operator entanglement for some regions in the Weyl chamber. First, the line $c_1 = c_2 = 0.5$, $c_3 < 0.5$ has the largest possible $s(\boldsymbol{c}) = 2 \log 2$ [50]. They are the building block of so-called dual-unitary circuits [61,62,68], which exhibit the fastest scrambling in the family of random circuits [63,64]. Recently, it was shown that after perturbing the dual-unitary point the gate operator entanglement plays a crucial role in recovering the more generic quantum chaotic behavior [69]. This motivates our choice to study dynamical signatures of the localization-delocalization transition as a function of the operator entanglement of the two-qubit gate they consist of.

The operator entanglement at any point of the Weyl chamber is given by [50]

$$s(\boldsymbol{c}) = -\ln[P(\boldsymbol{c})/32], \tag{6}$$

with

$$\begin{aligned} P(\boldsymbol{c}) = 14 &+ 4\cos(2\pi c_1) + 4\cos(2\pi c_2) + 4\cos(2\pi c_3) \\ &+ \cos[2\pi(c_1 - c_2)] + \cos[2\pi(c_1 + c_2)] \\ &+ \cos[2\pi(c_1 - c_3)] + \cos[2\pi(c_1 + c_3)] \\ &+ \cos[2\pi(c_2 + c_3)] + \cos[2\pi(c_2 - c_3)]. \end{aligned} \tag{7}$$

D. Level statistics and eigenstate entanglement entropy

The long-time dynamics of Floquet circuits can be probed by the spectral properties of the Floquet operator [8]. In particular, we are interested in the eigenphases and eigenstates $U|n\rangle = e^{i\theta_n}|n\rangle$. The gaps between consecutive eigenphases are defined as $\delta_i = \theta_{i+1} - \theta_i$, and the ratio between two consecutive gaps is denoted as

$$r_i = \min(\delta_{i+1}, \delta_i)/\max(\delta_{i+1}, \delta_i). \tag{8}$$

The average gap ratio r is known to serve as an order parameter for ergodicity-breaking transitions [21,70]: When the Floquet dynamics leads to thermalization, the mean gap ratio is described by Gaussian unitary ensemble (GUE) random matrix ensemble $\bar{r} \approx 0.60$ [71]. In contrast, when the Floquet dynamics gets localized, i.e., MBL, the gap ratio statistics is Poissonian such that $\bar{r} = 2\log 2 - 1 \approx 0.386$ [8,17]. If our Floquet model undergoes a MBL transition it should show up in the behavior of r as a function of the Schmidt coefficients.

A second diagnostic for the transition is the structure of eigenstates of the time-evolution operator: we introduce the reduced density matrix over half of the system as $\rho_A = \mathrm{Tr}_{L/2}(|n\rangle\langle n|)$. We probe the transition at the level of eigenstates using the half-chain entanglement entropy

$$S = -\mathrm{Tr}\rho_A \ln \rho_A. \tag{9}$$

In the thermal phase, the eigenstates are expected to be essentially random vectors in Hilbert space; thus their entanglement entropy is proportional to the chain length $S_{\mathrm{Page}} = (L\log 2 - 1)/2$, the so-called Page value [72]. On the other hand, in the localized phase the eigenstates only exhibit short-range entanglement, resulting in an area law for the entanglement entropy $S \approx \mathrm{const}$ [1]. Hence, the average entanglement entropy $\bar{S}$ signals the MBL transition [21,73,74].

These quantities are obtained using exact diagonalization. For small system sizes $L = 8, 10, 12$ the whole eigenspectrum is computed, while for larger system sizes $L \geqslant 14$ polynomial filtered diagonalization [75] is used for extracting 100 eigenpairs of the Floquet unitary. All quantities are averaged over 3000–6000 disorder realizations (except for $L = 20$ where only 500–1000 realizations are used) and all available eigenstates.

E. Quench dynamics

Another direct way to detect localization in our system is using transport properties. A common tool is the

autocorrelator [20,76–79]:

$$C(t) = \frac{1}{2^L}\mathrm{Tr}[\hat{O}(t)\hat{O}] = \frac{1}{2^L}\mathrm{Tr}[(\hat{U}^\dagger(t)\hat{O}\hat{U}(t)\hat{O}]. \tag{10}$$

Here O is a normalized observable with vanishing mean ($\mathrm{Tr}\hat{O} = 0$, $\mathrm{Tr}\hat{O}^2 = 2^L$), and the time evolution is generated by the circuit introduced in Eq. (3), i.e., $\hat{U}(t) = U(\boldsymbol{c})^t$.

Since our goal is to probe scrambling caused by the entangling gates, we choose an operator $\hat{O}$ such that $C(t) = 1$ for $c_1 = c_2 = c_3 = 0$. To achieve this, consider the product of the single-site operators at $i = \lfloor L/2 \rfloor$:

$$R = u_i w_i. \tag{11}$$

Since R is unitary, there exists a diagonal matrix D and a unitary V such that

$$R = V^\dagger D V. \tag{12}$$

By choosing

$$\hat{O} = V^\dagger \sigma_i^z V \tag{13}$$

we obtain an autocorrelator $C(t)$ with the desired properties. It is important to note that the choice of V depends on the specific disorder configuration. When the system thermalizes, the disorder-averaged autocorrelator vanishes in the long-time limit [1]. In contrast, $C(t)$ is expected to converge to a nonzero value in the MBL regime [1]. In summary, we obtain

$$\lim_{t\to\infty} C(t) = \begin{cases} 0, & \text{thermalization} \\ c > 0, & \text{localization.} \end{cases} \tag{14}$$

Another way to probe transport properties in the study of MBL is the entanglement entropy production starting from a product state $|\psi(0)\rangle = |\psi_0\rangle$ [41,80]. Analog to Sec. II D, we compute the half-chain entanglement entropy $S(t)$ [cf. Eq. (9)], but now for the time-evolved state $|\psi(t)\rangle$ instead. The entanglement growth rate depends on the overall dynamics: quantum chaotic systems show linear growth in time, while MBL systems exhibit logarithmic growth of entanglement [37,41]. The latest signals the existence of quasilocal integrals of motion [18,19].

III. RESULTS

A. Gap ratio and eigenstate entanglement entropy

As a first check, we probe the operator entanglement per gate $s(\boldsymbol{c})$ as a unifying parameter for the interaction strength. To do so, we show the gap ratio and the eigenstate entanglement entropy as a function of the gate entanglement entropy $s(\boldsymbol{c})$ in Figs. 3(a) and 3(b), respectively. We focus on parameters $\boldsymbol{c}(c_1, c_2, c_3)$ within the range $c_1, c_2 = [0.02, 0.28]$ and $c_3 = [0.0, 0.18]$. For the system size and $s(\boldsymbol{c})$ fixed, the gap ratio and half-chain entanglement almost collapse on top of the corresponding SWAP line value. This supports our motivation to choose $s(\boldsymbol{c})$ as an indicator for the interaction strength.

However, the results for the CNOT and the SWAP line lie not directly on top of each other. This difference may originate from the specific choice of the vector $\boldsymbol{c}$. On the CNOT line, two Schmidt coefficients λ_l [cf. Eq. (8)] are zero [50], which is not the case for any other choice of $\boldsymbol{c}$ in the Weyl chamber.

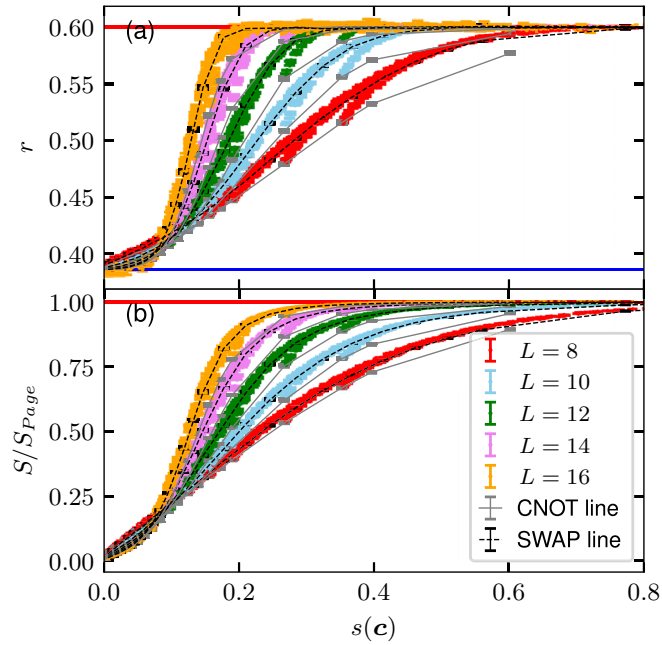

FIG. 3. Gap ratio (a) and eigenstate entanglement entropy (b) for system sizes $L = 8, 10, 12, 14, 16$ and combination of values: $c_1, c_2 = 0.02, 0.04, 0.06, \ldots, 0.2, 0.24, 0.28$ and $c_3 = 0, 0.02, 0.04, \ldots, 0.18$. SWAP line (black dashed) and CNOT line (gray continuous) are also shown for comparison. Error bars are 68% confidence interval.

Therefore, the finite-size behavior visible in r and S/S_{Page} may be affected by this choice of $\boldsymbol{c}$ (see Appendix A for a more quantitative comparison).

For our further studies, we choose three parameter lines that differ in the number of nonvanishing coefficients c_i: the SWAP line, the iSWAP line, and the CNOT line (cf. Sec. II B). The gap ratio and the half-chain entanglement entropy on these lines of the Weyl chamber and systems sizes are shown in Fig. 4. In all three cases, we see a crossover between an MBL regime (indicated by a small eigenstate entanglement entropy and an r value close to the Poissonian case) for small interactions towards a thermal regime at large interactions.

The curves of different system sizes intersect. Analogously to Refs. [17,21,26], we then compare the different crossings between consecutive system sizes to check the stability of the phase in the thermodynamic limit [70]. In Fig. 5, the crossings of gap ratio and entanglement entropy for consecutive sizes L and $L + 2$ are shown. The trend of the crossing suggests a scaling $\propto 1/L$, at least for the accessible system sizes. Remarkably, finite-size effects for the half-chain entanglement entropy are less pronounced in comparison to the r value. The trend of the data suggests that the crossings are shifting towards zero in the limit $L \to \infty$, thus ergodicity is restored at any finite interaction. However, given the smallness of the accessible system sizes, we can not rule out a change in the trend at larger sizes.

Finally, we present an analysis of the entanglement entropy fluctuations of the Floquet eigenstates. It is known that fluctuations around the mean eigenstate entanglement entropy $\overline{S}$, probed by $\sigma_S^2 = \overline{S^2} - \overline{S}^2$, peak at the transition

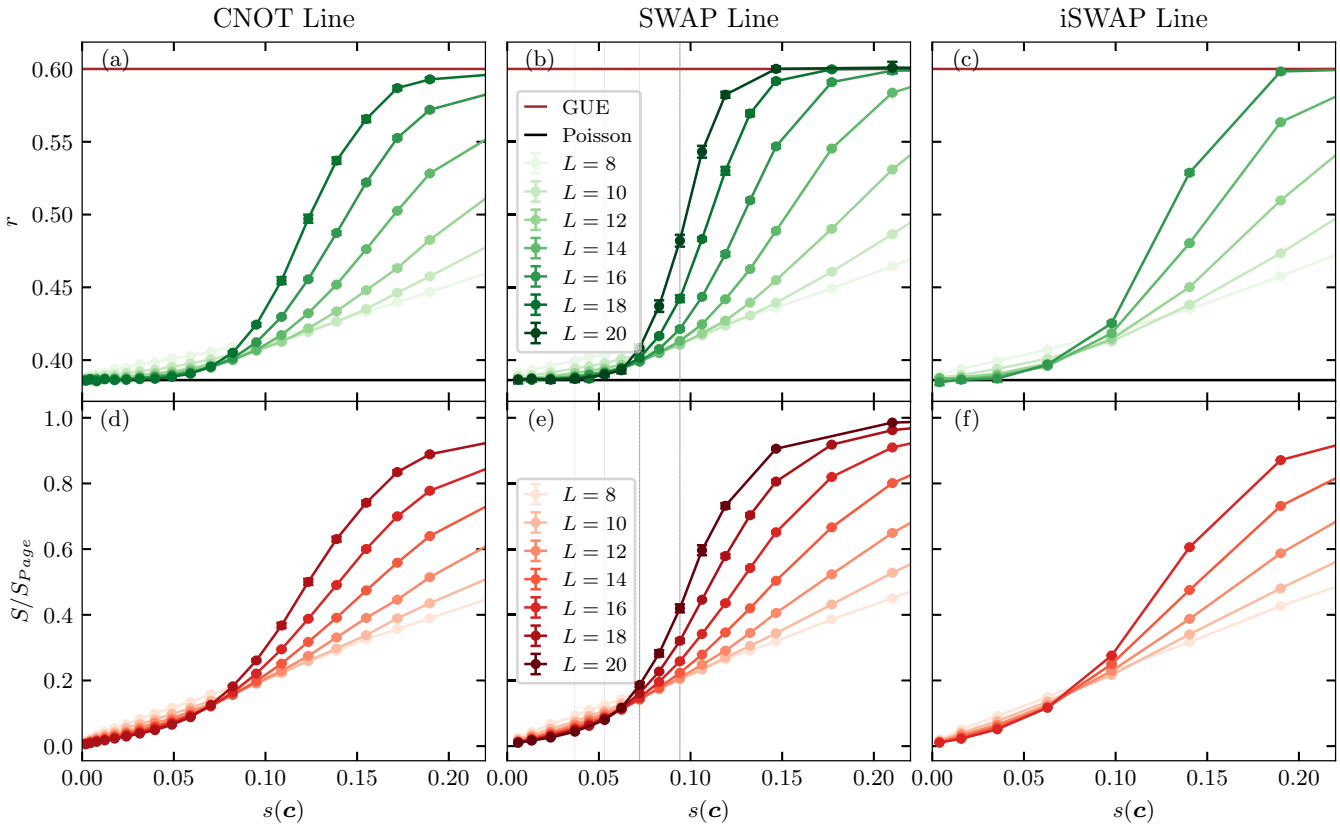

FIG. 4. Upper row (a)–(c): Gap ratio as function of the two-qubit-gate operator entanglement entropy for system sizes $L = 8, 10, 12, 14, 16$ (in addition CNOT line has $L = 18$ and SWAP line has $L = 18, 20$). Lower row (d)–(f): Average entanglement entropy normalized by the Page value $S_{\text{Page}} = 0.5(L \log 2 - 1)$ for the same system sizes. Right column: CNOT line denoted by $c_1 \in [0.02, 0.40]$, $c_2 = c_3 = 0$. Middle column: SWAP line denoted as $c_1 = c_2 = c_3$ with $c_1 \in [0.02, 0.40]$. Left column: iSWAP line denoted by $c_2 = c_1$, $c_3 = 0$ and $c_1 \in [0.02, 0.28]$. Error bars (too small for this scale) are 68% confidence interval. Gray vertical lines are the $s(\boldsymbol{c})$ for which dynamics is shown in Sec. III B. In all three cases, the operator entanglement entropy $s(\boldsymbol{c})$ indicates an MBL-to-thermal crossover for both gap ratio and eigenstate entanglement entropy.

point [21] and thus are a good indicator to identify the delocalization-localization transition [80,81]. Such fluctuations are shown in Fig. 6. We see that the peak of the fluctuations is moving towards smaller $s(\boldsymbol{c})$, as has been reported in other models where MBL might be stable [74].

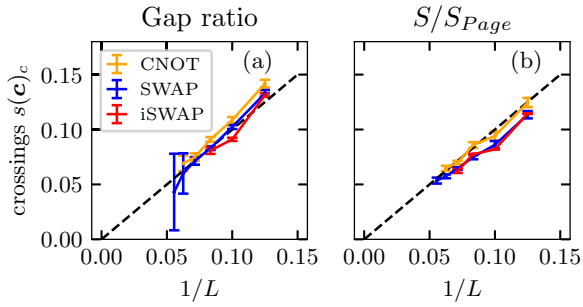

FIG. 5. Crossings of the curves in Fig. 4 between system sizes L and $L + 2$ for the gap ratio (a) and eigenstate entanglement entropy (b) along the CNOT line (orange), SWAP line (blue), iSWAP line (red). The black dashed lines show the scaling $1/L$. For accessible system sizes the trend is compatible within error bars with $s(\boldsymbol{c})_c \propto 1/L$, suggesting restoring of ergodicity in the thermodynamic limit for any finite interaction strength.

Importantly, the entanglement entropy fluctuations also seem to be sensitive only to the operator entanglement $s(\boldsymbol{c})$ of the gate rather than the specific choice (c_1, c_2, c_3) in the Weyl chamber.

B. Single-spin autocorrelation and entanglement entropy after a quench

From the previous section, we can conclude that the critical operator entanglement per gate $s(\boldsymbol{c})$ is scaling roughly as $1/L$. The largest system size for which we could extract eigenvalues and eigenvectors is $L = 20$. From Fig. 5, we estimate the crossover region for current system sizes to be around $s(\boldsymbol{c}) \sim 1/20 = 0.05$. In this section, we explore signatures for this crossover in quench dynamics for up to 10^5 cycles in the regime $s(\boldsymbol{c}) \lesssim 0.1$ and system sizes $L \geqslant 18$.

In Fig. 7, we show the autocorrelation function introduced in Sec. II E on the SWAP line of the model. The circuit dynamics is simulated using CIRQ [82] that allows to reach 10^5 cycles and up to $L = 22$ qubits.

For $s(\boldsymbol{c}) \approx 0.09, 0.07$ close to the crossover region, $\overline{C}(t)$ decays with a scale either logarithmically or stretched exponentially, in line with previous work on autocorrelation decay in prethermal systems [76]. The long-time limit $\lim_{t\to\infty} C(t)$ decreases with system size, suggesting a

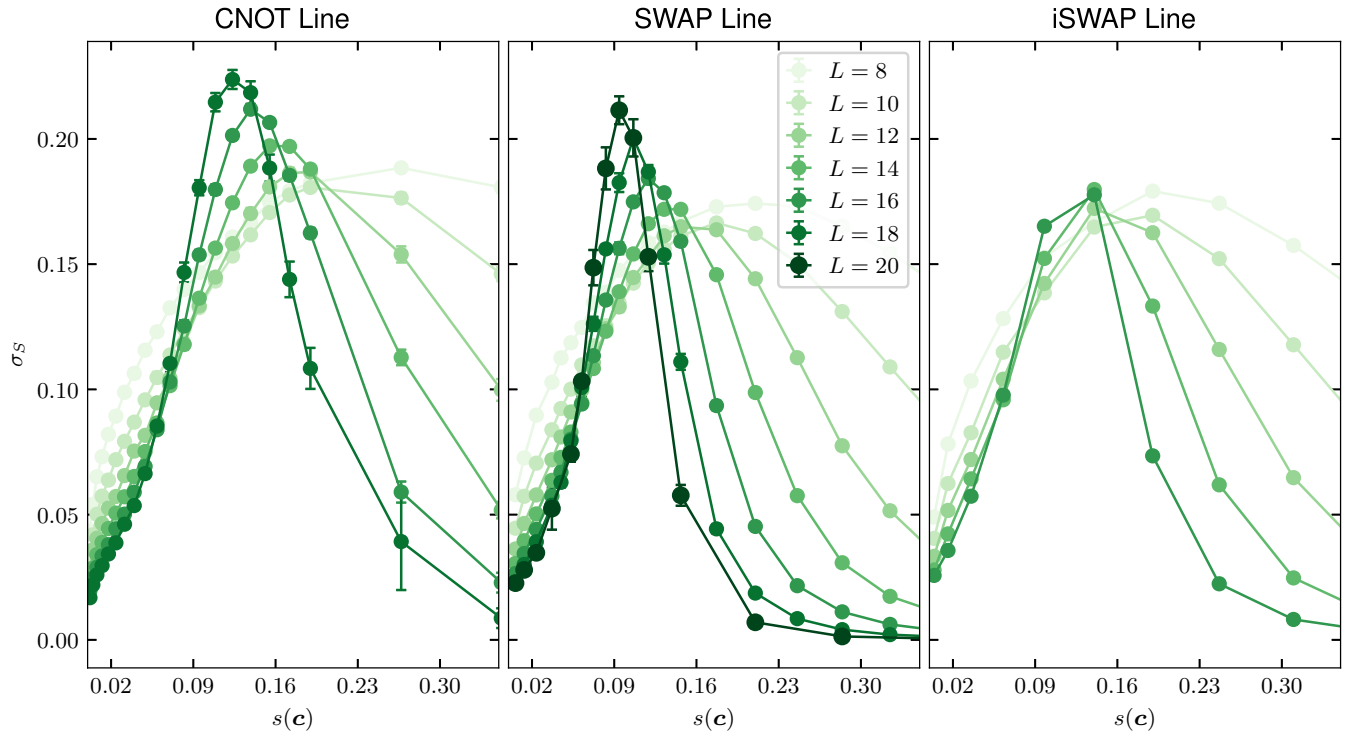

FIG. 6. Entanglement entropy fluctuations $\sigma_S^2 = \overline{s^2} - \overline{s}^2$ with $s = S/S_{\text{Page}}$ as function of the two-qubit gate operator entanglement. Right column: CNOT line denoted by $c_1 \in [0.02, 0.40]$. Middle column: SWAP line with $c_1 \in [0.02, 0.40]$. Left column: iSWAP line with $c_1 \in [0.02, 0.28]$. Error bars (too small for this scale) are 68% confidence interval. The data set is the same shown in Fig. 4 for S/S_{Page}.

trend towards thermalization. For smaller interactions $s(\boldsymbol{c}) \approx 0.05, 0.03$, our accessible timescales are too short to draw conclusions about a drift in the long-time dynamics: we do not reach a steady state in our numerics.

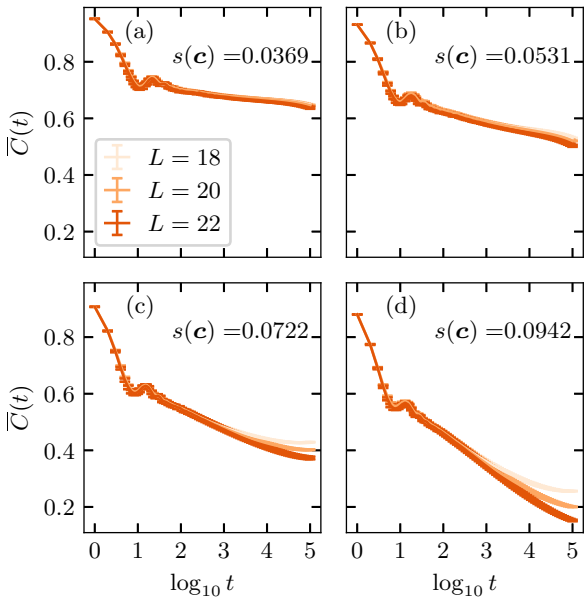

FIG. 7. Single-spin autocorrelation $\overline{C}(t)$ as a function of time t, gates $G(\boldsymbol{c})$ are chosen on the SWAP line for $c = (0.05, 0.06, 0.07, 0.08)$ [the corresponding interaction strength $s(\boldsymbol{c})$ is shown in each panel]. Disorder average is taken over 1000–4000 disorder realizations. Errors bars are 68% confidence interval.

Finally, we study the entanglement entropy growth for initial product states along the SWAP line. As discussed in Sec. II E, a signature of localization is logarithmic entanglement growth. As is visible in Fig. 8, the entanglement entropy $S(t)$ is growing faster than logarithmically (black dashed lines) at timescales $t \gtrsim 10^3$ and interactions $s(\boldsymbol{c}) \gtrsim 0.07$. In order to confirm this observation, we compute the derivative of $S(t)$ with respect to $\ln t$ (see Fig. 9). A logarithmic curve would be visible as a constant value. Instead, we see that the derivative keeps growing with system size even in the regime when the level statistics is Poissonian $s(c) = 0.0369$. We conclude that the entropy growth is faster than pure logarithmic growth even for the smallest interactions. The latest is in odds with the steady logarithmic growth in MBL regimes [37].

IV. DISCUSSION

In this work, we have introduced a generic Floquet circuit model that allows us to parametrically tune the interaction and keep the disorder maximal. We have identified the gate entanglement entropy $s(\boldsymbol{c})$ as a quantitative measure for the interaction. In the limit $s(\boldsymbol{c}) = 0$, our model reduces to a non-interacting system. Our results for various quantities suggest that the observed MBL regime for small interactions does not persist in the thermodynamic limit.

Our reachable system sizes and our investigated model are not sufficient to draw conclusions about the general fate of the MBL transition in the thermodynamic limit. Nevertheless, they suggest analyzing whether the results for

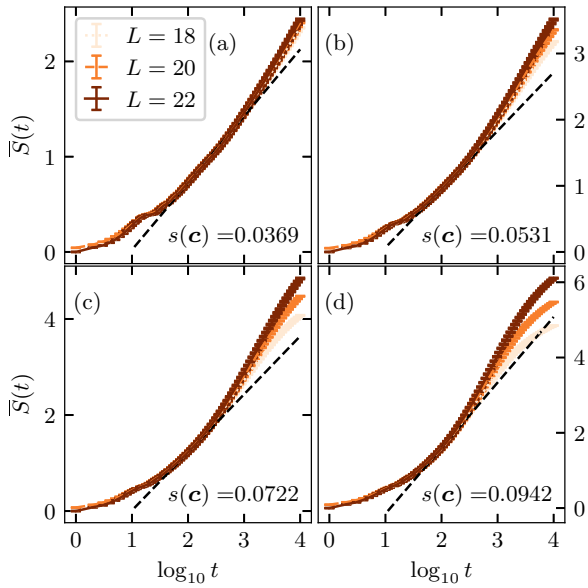

FIG. 8. Half-chain entanglement entropy after a quench on the SWAP line for $c = (0.05, 0.06, 0.07, 0.08)$ [same values but translated to $s(\boldsymbol{c})$ are shown in each panel] and system sizes $L = 18, 20, 22$. Disorder average is taken over 1000–4000 disorder realizations, error bars denote 68% confidence interval. The black dashed lines denote a fit $a \ln t + b$ for comparison, with a determined by the derivative of the $L = 22$ curve at $t = 10^3$. For large interactions $S(t)$ the logarithmic growth is proceeded by a faster entanglement entropy growth.

other commonly studied models in the field of many-body localization are in alignment with an integrability-breaking transition [36,83] instead.

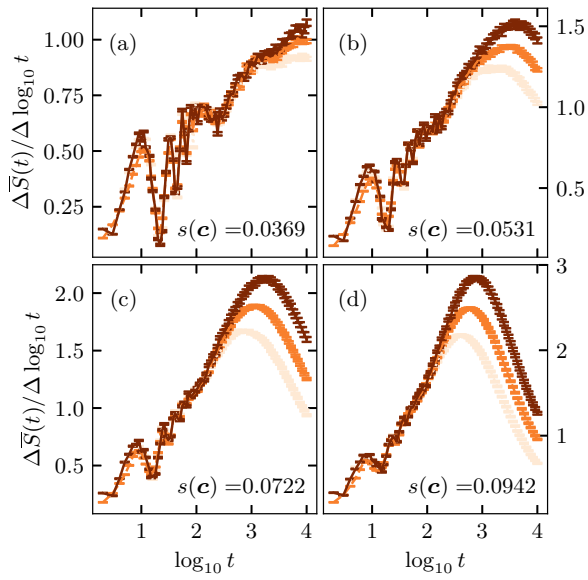

FIG. 9. Numerical derivative of the half-chain entanglement entropy with respect to $\ln t$ after a quench on the SWAP line for $c = (0.05, 0.06, 0.07, 0.08)$ (same data are shown in Fig. 8) and system sizes $L = 18, 20, 22$. The entropy growth is faster than pure logarithmic for all interaction strengths.

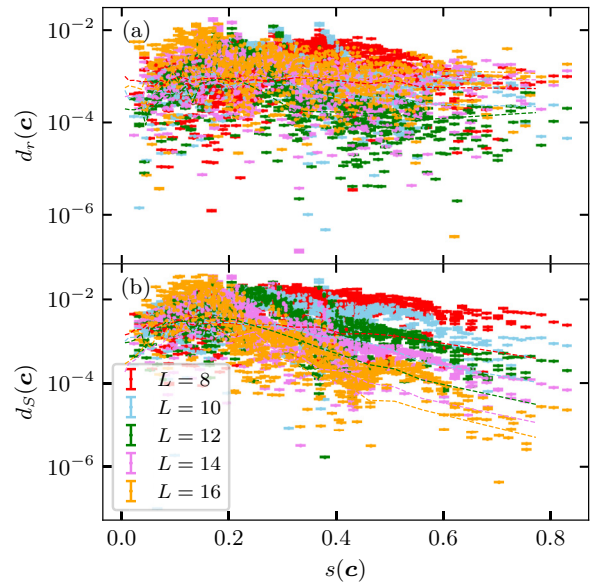

FIG. 10. Distance of (a) the gap ratio $r(\boldsymbol{c}, L)$ and (b) entanglement entropy $S(\boldsymbol{c}, L)$ to the reference values $r(\boldsymbol{c}_S, L)$ and $S(\boldsymbol{c}_S, L)$ on the SWAP line. Dashed lines are error bars of $r(\boldsymbol{c}_S, L)$ and $S(\boldsymbol{c}_S, L)$. The SWAP reference points are computed by using spline interpolation of the curves shown in Fig. 4. The points are the same data as shown in Fig. 3.

Moreover, it is an interesting question to establish connections between this model, where both direction and strength are subjected to disorder, and models where the direction of the single-qubit unitaries is fixed. The XXZ spin chain and its variants are part of the latter. Furthermore, the effect of spatial variations on the gate operator entanglement can give rise to "slow" and "fast" dynamical regions very much in the spirit of quantum avalanches proposed as delocalization mechanism [34,35]. The investigation of the role of both types of disorder and the effects of spatial fluctuations in gate operator entanglement are both interesting venues for future research.

Apart from that, our model contains dual-unitary circuits as another special case for a specific choice of parameters $\boldsymbol{c}$. This model is thus a good starting point to study the effects of breaking dual unitarity in more detail [69].

ACKNOWLEDGMENTS

We thank A. Chandran, P. Claeys, D. Long, D. Luitz, and M. Rampp for inspiring discussions. L.C. gratefully acknowledges funding by the U.S. ARO Grant No. W911NF-21-1-0007. All statements of fact, opinion or conclusions contained herein are those of the authors and should not be construed as representing the official views or policies of the U.S. Government.

APPENDIX A: GATE OPERATOR ENTANGLEMENT, SWAP, AND CNOT LINES

Throughout this work, we assume that the results for the SWAP, iSWAP, and CNOT line can be extrapolated to any other set of $\boldsymbol{c} = (c_1, c_2, c_3)$ via the equivalence through the gate operator entanglement $s(\boldsymbol{c})$. Inspired by Ref. [69], where

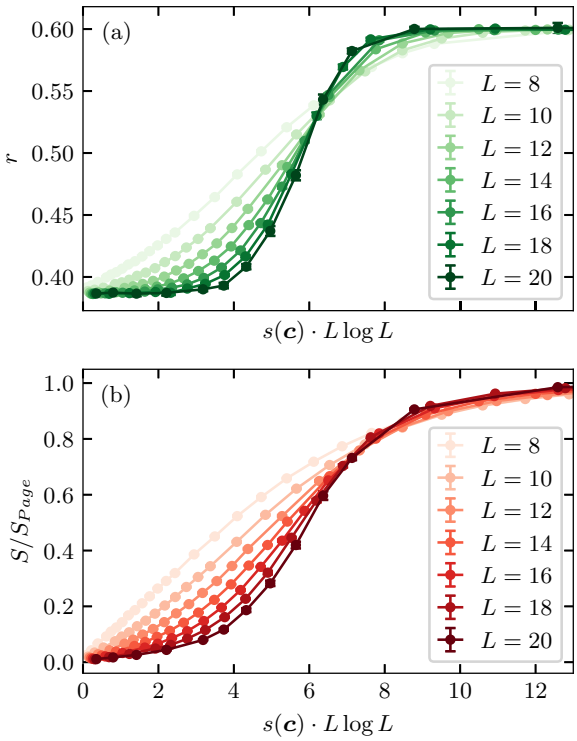

FIG. 11. (a) Gap ratio and (b) entanglement entropy along the SWAP line for system size $L = 8$–20. The two-qubit gate operator entanglement $s(\boldsymbol{c})$ is rescaled by $L \ln L$. The data set is the same as shown in Fig. 4. These visible crossings suggest a drifting critical value $s(\boldsymbol{c})_{\text{crit}} \propto 1/L$, compatible with an integrability-breaking phenomenon (see Appendix B).

the authors found that $s(\boldsymbol{c})$ plays a leading role in generic thermalization, we aim to apply these ideas to the weakly interacting regime. In this Appendix, we provide quantitative tests for this assumption by computing the gap ratio and eigenstate operator entanglement at any point (c_1, c_2, c_3), namely, $r(\boldsymbol{c}, L)$ and $S(\boldsymbol{c}, L)$, and the difference

$$d_r(\boldsymbol{c}) = |r(\boldsymbol{c}, L) - r(\boldsymbol{c}_S, L)| \tag{A1}$$

$$d_S(\boldsymbol{c}) = |S(\boldsymbol{c}, L) - S(\boldsymbol{c}_S, L)|/S_{\text{Page}}, \tag{A2}$$

where $r(\boldsymbol{c}_S, L)$ and $S(\boldsymbol{c}_S, L)$ are the gap ratio and eigenstate entanglement entropy for the reference choice $\boldsymbol{c}_S = (c_x, c_x, c_x)$ on the SWAP line and the same gate operator entanglement entropy $s(\boldsymbol{c}) = s(\boldsymbol{c}_S)$. Our results are shown in Fig. 10. As a reference, we compare these results with the effects of the statistical error of $r(\boldsymbol{c}_S, L)$ and $S(\boldsymbol{c}_S, L)$ due to the disorder average, indicated by dashed lines. When a point $d_r(\boldsymbol{c})$ or $d_S(\boldsymbol{c})$ is below the corresponding error bar line, then the difference of the results for the parameter $\boldsymbol{c}$ and the reference point $\boldsymbol{c}_S$ is the same within statistical errors. Visually, there is a large fraction of $d_r(\boldsymbol{c})$ or $d_S(\boldsymbol{c})$ above the error bar line for all system sizes. However, the difference in absolute value is small enough, such that extrapolating the results from the SWAP, iSWAP, and CNOT line to other values of $\boldsymbol{c}$ is a fair assumption for the current setup and system sizes.

APPENDIX B: COMPARISON WITH SCALING OF INTEGRABILITY-BREAKING PERTURBATIONS

It has been recently shown that noninteracting spin systems with small perturbative interaction undergo a Fock-space-type delocalization "transition" that marks the onset of quantum chaos [43]. Taking ϵ as the integrability-breaking parameter, the value ϵ_c denotes the onset of chaos scaling as $\epsilon_c \sim (L \ln L)^{-1}$ with increasing system size. In Fig. 11 we test such scaling for $s(\boldsymbol{c})$ for both gap ratio and eigenstate entanglement entropy. Although the available system sizes do not allow us to discern the $\ln L$ component, the linear scaling is clearly visible. From this perspective, the MBL-thermalization crossover appears to have a similar scaling as an integrability-breaking phenomenon for finite system sizes.

[1] R. Nandkishore and D. A. Huse, Many-body localization and thermalization in quantum statistical mechanics, Annu. Rev. Condens. Matter Phys. **6**, 15 (2015).
[2] D. A. Abanin, E. Altman, I. Bloch, and M. Serbyn, *Colloquium:* Many-body localization, thermalization, and entanglement, Rev. Mod. Phys. **91**, 021001 (2019).
[3] M. Ueda, Quantum equilibration, thermalization and prethermalization in ultracold atoms, Nat. Rev. Phys. **2**, 669 (2020).
[4] J. M. Deutsch, Quantum statistical mechanics in a closed system, Phys. Rev. A **43**, 2046 (1991).
[5] M. Srednicki, Chaos and quantum thermalization, Phys. Rev. E **50**, 888 (1994).
[6] M. Rigol, V. Dunjko, and M. Olshanii, Thermalization and its mechanism for generic isolated quantum systems, Nature (London) **452**, 854 (2008).
[7] E. J. Heller, Quantum chaos: An introduction, Phys. Today **54**(1), 49 (2001).
[8] L. D'Alessio, Y. Kafri, A. Polkovnikov, and M. Rigol, From quantum chaos and eigenstate thermalization to statistical mechanics and thermodynamics, Adv. Phys. **65**, 239 (2016).
[9] P. W. Anderson, Absence of diffusion in certain random lattices, Phys. Rev. **109**, 1492 (1958).
[10] L. Vidmar and M. Rigol, Generalized gibbs ensemble in integrable lattice models, J. Stat. Mech. (2016) 064007.
[11] M. Brenes, T. LeBlond, J. Goold, and M. Rigol, Eigenstate thermalization in a locally perturbed integrable system, Phys. Rev. Lett. **125**, 070605 (2020).
[12] M. Rigol, Fundamental asymmetry in quenches between integrable and nonintegrable systems, Phys. Rev. Lett. **116**, 100601 (2016).
[13] F. H. L. Essler and M. Fagotti, Quench dynamics and relaxation in isolated integrable quantum spin chains, J. Stat. Mech. (2016) 064002.
[14] M. Rigol, V. Dunjko, V. Yurovsky, and M. Olshanii, Relaxation in a completely integrable many-body quantum system: An *ab initio* study of the dynamics of the highly excited states of 1D lattice hard-core bosons, Phys. Rev. Lett. **98**, 050405 (2007).

[15] D. M. Basko, I. L. Aleiner, and B. L. Altshuler, Metalinsulator transition in a weakly interacting many-electron system with localized single-particle states, Ann. Phys. **321**, 1126 (2006).
[16] I. V. Gornyi, A. D. Mirlin, and D. G. Polyakov, Interacting electrons in disordered wires: Anderson localization and low-T transport, Phys. Rev. Lett. **95**, 206603 (2005).
[17] V. Oganesyan and D. A. Huse, Localization of interacting fermions at high temperature, Phys. Rev. B **75**, 155111 (2007).
[18] D. A. Huse, R. Nandkishore, and V. Oganesyan, Phenomenology of fully many-body-localized systems, Phys. Rev. B **90**, 174202 (2014).
[19] M. Serbyn, Z. Papic, and D. A. Abanin, Local conservation laws and the structure of the many-body localized states, Phys. Rev. Lett. **111**, 127201 (2013).
[20] M. Schreiber, S. S. Hodgman, P. Bordia, H. P. Lüschen, M. H. Fischer, R. Vosk, E. Altman, U. Schneider, and I. Bloch, Observation of many-body localization of interacting fermions in a quasirandom optical lattice, Science **349**, 842 (2015).
[21] D. J. Luitz, N. Laflorencie, and F. Alet, Many-body localization edge in the random-field Heisenberg chain, Phys. Rev. B **91**, 081103(R) (2015).
[22] J. Suntajs, J. Bonča, T. Prosen, and L. Vidmar, Quantum chaos challenges many-body localization, Phys. Rev. E **102**, 062144 (2020).
[23] D. Sels and A. Polkovnikov, Thermalization of dilute impurities in one-dimensional spin chains, Phys. Rev. X **13**, 011041 (2023).
[24] D. Sels and A. Polkovnikov, Dynamical obstruction to localization in a disordered spin chain, Phys. Rev. E **104**, 054105 (2021).
[25] M. Kiefer-Emmanouilidis, R. Unanyan, M. Fleischhauer, and J. Sirker, Slow delocalization of particles in many-body localized phases, Phys. Rev. B **103**, 024203 (2021).
[26] A. Morningstar, L. Colmenarez, V. Khemani, D. J. Luitz, and D. A. Huse, Avalanches and many-body resonances in many-body localized systems, Phys. Rev. B **105**, 174205 (2022).
[27] D. Sels, Bath-induced delocalization in interacting disordered spin chains, Phys. Rev. B **106**, L020202 (2022).
[28] P. J. D. Crowley and A. Chandran, Avalanche induced coexisting localized and thermal regions in disordered chains, Phys. Rev. Res. **2**, 033262 (2020).
[29] P. Sierant and J. Zakrzewski, Challenges to observation of many-body localization, Phys. Rev. B **105**, 224203 (2022).
[30] P. Sierant, D. Delande, and J. Zakrzewski, Thouless time analysis of Anderson and many-body localization transitions, Phys. Rev. Lett. **124**, 186601 (2020).
[31] R. K. Panda, A. Scardicchio, M. Schulz, S. R. Taylor, and M. Nidari, Can we study the many-body localisation transition? Europhys. Lett. **128**, 67003 (2020).
[32] P. Crowley and A. Chandran, A constructive theory of the numerically accessible many-body localized to thermal crossover, SciPost Phys. **12**, 201 (2022).
[33] N. Laflorencie, G. Lemarie, and N. Mace, Topological order in random interacting Ising-Majorana chains stabilized by many-body localization, Phys. Rev. Res. **4**, L032016 (2022).
[34] W. De Roeck and J. Z. Imbrie, Many-body localization: stability and instability, Philos. Trans. R. Soc. London A **375**, 20160422 (2017).
[35] T. Thiery, F. Huveneers, M. Muller, and W. De Roeck, Many-body delocalization as a quantum avalanche, Phys. Rev. Lett. **121**, 140601 (2018).
[36] B. Krajewski, L. Vidmar, J. Bonča, and M. Mierzejewski, Restoring ergodicity in a strongly disordered interacting chain, Phys. Rev. Lett. **129**, 260601 (2022).
[37] J. H. Bardarson, F. Pollmann, and J. E. Moore, Unbounded growth of entanglement in models of many-body localization, Phys. Rev. Lett. **109**, 017202 (2012).
[38] M. Serbyn and J. E. Moore, Spectral statistics across the many-body localization transition, Phys. Rev. B **93**, 041424(R) (2016).
[39] S. Ray, A. Ghosh, and S. Sinha, Drive-induced delocalization in the Aubry-André model, Phys. Rev. E **97**, 010101(R) (2018).
[40] A. Lazarides, A. Das, and R. Moessner, Fate of many-body localization under periodic driving, Phys. Rev. Lett. **115**, 030402 (2015).
[41] M. Znidaric, T. Prosen, and P. Prelovsek, Many-body localization in the Heisenberg *XXZ* magnet in a random field, Phys. Rev. B **77**, 064426 (2008).
[42] P. Sierant, M. Lewenstein, A. Scardicchio, and J. Zakrzewski, Stability of many-body localization in Floquet systems, Phys. Rev. B **107**, 115132 (2023).
[43] V. B. Bulchandani, D. A. Huse, and S. Gopalakrishnan, Onset of many-body quantum chaos due to breaking integrability, Phys. Rev. B **105**, 214308 (2022).
[44] B. Kraus and J. I. Cirac, Optimal creation of entanglement using a two-qubit gate, Phys. Rev. A **63**, 062309 (2001).
[45] S. Balakrishnan and R. Sankaranarayanan, Measures of operator entanglement of two-qubit gates, Phys. Rev. A **83**, 062320 (2011).
[46] S. Balakrishnan and R. Sankaranarayanan, Entangling power and local invariants of two-qubit gates, Phys. Rev. A **82**, 034301 (2010).
[47] S. Balakrishnan and R. Sankaranarayanan, Characterizing the geometrical edges of nonlocal two-qubit gates, Phys. Rev. A **79**, 052339 (2009).
[48] J. Zhang, J. Vala, S. Sastry, and K. B. Whaley, Geometric theory of nonlocal two-qubit operations, Phys. Rev. A **67**, 042313 (2003).
[49] Y. Makhlin, Nonlocal properties of two-qubit gates and mixed states, and the optimization of quantum computations, Quantum Inf. Proc. **1**, 243 (2002).
[50] S. Balakrishnan and R. Sankaranarayanan, Operator-schmidt decomposition and the geometrical edges of two-qubit gates, Quantum Inf. Proc. **10**, 449 (2011).
[51] B. Bertini, P. Kos, and T. Prosen, Exact correlation functions for dual-unitary lattice models in 1 + 1 dimensions, Phys. Rev. Lett. **123**, 210601 (2019).
[52] M. P. A. Fisher, V. Khemani, A. Nahum, and S. Vijay, Random quantum circuits, Annu. Rev. Condens. Matter Phys. **14**, 335 (2023).
[53] L. Piroli, B. Bertini, J. I. Cirac, and T. Prosen, Exact dynamics in dual-unitary quantum circuits, Phys. Rev. B **101**, 094304 (2020).
[54] B. Bertini, P. Kos, and T. Prosen, Operator entanglement in local quantum circuits I: Chaotic dual-unitary circuits, SciPost Phys. **8**, 067 (2020).

[55] B. Bertini, P. Kos, and T. Prosen, Operator entanglement in local quantum circuits II: Solitons in chains of qubits, SciPost Phys. **8**, 068 (2020).

[56] P. W. Claeys and A. Lamacraft, Ergodic and nonergodic dual-unitary quantum circuits with arbitrary local hilbert space dimension, Phys. Rev. Lett. **126**, 100603 (2021).

[57] S. Aravinda, S. A. Rather, and A. Lakshminarayan, From dual-unitary to quantum Bernoulli circuits: Role of the entangling power in constructing a quantum ergodic hierarchy, Phys. Rev. Res. **3**, 043034 (2021).

[58] B. Bertini, P. Kos, and T. Prosen, Random matrix spectral form factor of dual-unitary quantum circuits, Commun. Math. Phys. **387**, 597 (2021).

[59] B. Bertini, P. Kos, and T. Prosen, Exact spectral form factor in a minimal model of many-body quantum chaos, Phys. Rev. Lett. **121**, 264101 (2018).

[60] M. Borsi and B. Pozsgay, Construction and the ergodicity properties of dual unitary quantum circuits, Phys. Rev. B **106**, 014302 (2022).

[61] B. Bertini, P. Kos, and T. Prosen, Entanglement spreading in a minimal model of maximal many-body quantum chaos, Phys. Rev. X **9**, 021033 (2019).

[62] B. Bertini and L. Piroli, Scrambling in random unitary circuits: Exact results, Phys. Rev. B **102**, 064305 (2020).

[63] T. Zhou and A. W. Harrow, Maximal entanglement velocity implies dual unitarity, Phys. Rev. B **106**, L201104 (2022).

[64] J. Bensa and M. Žnidarič, Fastest local entanglement scrambler, multistage thermalization, and a non-Hermitian phantom, Phys. Rev. X **11**, 031019 (2021).

[65] F. Alet and N. Laflorencie, Many-body localization: An introduction and selected topics, C. R. Phys. **19**, 498 (2018).

[66] B. Foxen, C. Neill, A. Dunsworth, P. Roushan, B. Chiaro, A. Megrant, J. Kelly, Z. Chen, K. Satzinger, R. Barends, F. Arute, K. Arya, R. Babbush, D. Bacon, J. C. Bardin, S. Boixo, D. Buell, B. Burkett, Y. Chen, R. Collins, and J. M. Martinis, Demonstrating a continuous set of two-qubit gates for near-term quantum algorithms, Phys. Rev. Lett. **125**, 120504 (2020).

[67] S. J. Garratt and J. T. Chalker, Many-body delocalization as symmetry breaking, Phys. Rev. Lett. **127**, 026802 (2021).

[68] M. Akila, D. Waltner, B. Gutkin, and T. Guhr, Particle-time duality in the kicked Ising spin chain, J. Phys. A: Math. Theor. **49**, 375101 (2016).

[69] M. A. Rampp, R. Moessner, and P. W. Claeys, From dual unitarity to generic quantum operator spreading, Phys. Rev. Lett. **130**, 130402 (2023).

[70] A. Pal and D. A. Huse, Many-body localization phase transition, Phys. Rev. B **82**, 174411 (2010).

[71] Y. Y. Atas, E. Bogomolny, O. Giraud, and G. Roux, Distribution of the ratio of consecutive level spacings in random matrix ensembles, Phys. Rev. Lett. **110**, 084101 (2013).

[72] D. N. Page, Average entropy of a subsystem, Phys. Rev. Lett. **71**, 1291 (1993).

[73] V. Khemani, S. P. Lim, D. N. Sheng, and D. A. Huse, Critical properties of the many-body localization transition, Phys. Rev. X **7**, 021013 (2017).

[74] X. Yu, D. J. Luitz, and B. K. Clark, Bimodal entanglement entropy distribution in the many-body localization transition, Phys. Rev. B **94**, 184202 (2016).

[75] D. J. Luitz, Polynomial filter diagonalization of large Floquet unitary operators, SciPost Phys. **11**, 021 (2021).

[76] D. M. Long, P. J. D. Crowley, V. Khemani, and A. Chandran, Phenomenology of the prethermal many-body localized regime, Phys. Rev. Lett. **131**, 106301 (2023).

[77] D. J. Luitz, N. Laflorencie, and F. Alet, Extended slow dynamical regime close to the many-body localization transition, Phys. Rev. B **93**, 060201(R) (2016).

[78] T. L. M. Lezama, S. Bera, and J. H. Bardarson, Apparent slow dynamics in the ergodic phase of a driven many-body localized system without extensive conserved quantities, Phys. Rev. B **99**, 161106(R) (2019).

[79] T. L. M. Lezama, E. J. Torres-Herrera, F. Perez-Bernal, Y. BarLev, and L. F. Santos, Equilibration time in many-body quantum systems, Phys. Rev. B **104**, 085117 (2021).

[80] J. A. Kjall, J. H. Bardarson, and F. Pollmann, Many-body localization in a disordered quantum Ising chain, Phys. Rev. Lett. **113**, 107204 (2014).

[81] P. Ponte, Z. Papić, F. Huveneers, and D. A. Abanin, Many-body localization in periodically driven systems, Phys. Rev. Lett. **114**, 140401 (2015).

[82] C. Developers, CIRQ, see full list of authors on Github: https://github.com/quantumlib/Cirq/graphs/contributors.

[83] B. Krajewski, L. Vidmar, J. Bonča, and M. Mierzejewski, Strongly disordered anderson insulator chains with generic two-body interaction, Phys. Rev. B **108**, 064203 (2023).